Electronic Supplementary Material (ESI) for Nanoscale.
This journal is © The Royal Society of Chemistry 2024

Supplementary Material

Easily constructed porous silver films for efficient catalytic CO_2 reduction and Zn-CO_2 batteries

Junyang Ding[a], Tianran Wei[b], Tong Hou[b], Weijia Liu[b], Qian Liu[c], Hao Zhang[a], Jun Luo[d], and Xijun Liu[b]**

[a] Institute for New Energy Materials & Low-Carbon Technologies, School of Materials Science and Engineering, Tianjin University of Technology, Tianjin 300384, China

[b] State Key Laboratory of Featured Metal Materials and Life-cycle Safety for Composite Structures, Guangxi Key Laboratory of Processing for Non-ferrous Metals and Featured Materials, MOE Key Laboratory of New Processing Technology for Nonferrous Metals and Materials, School of Resources, Environment and Materials, Guangxi University, Nanning, 530004 Guangxi, China

[c] Institute for Advanced Study, Chengdu University, Chengdu 610106, Sichuan, China

[d] ShenSi Lab, Shenzhen Institute for Advanced Study, University of Electronic Science and Technology of China, Longhua District, Shenzhen 518110, China

***E-mail:** xjliu@gxu.edu.cn; ho.zhang@foxmail.com

Figures and Table

Figure S1. The optical photos of the as-prepared samples (from left to right: CP, Ag/CP, SBA-15/Ag/CP, and p-Ag/CP).

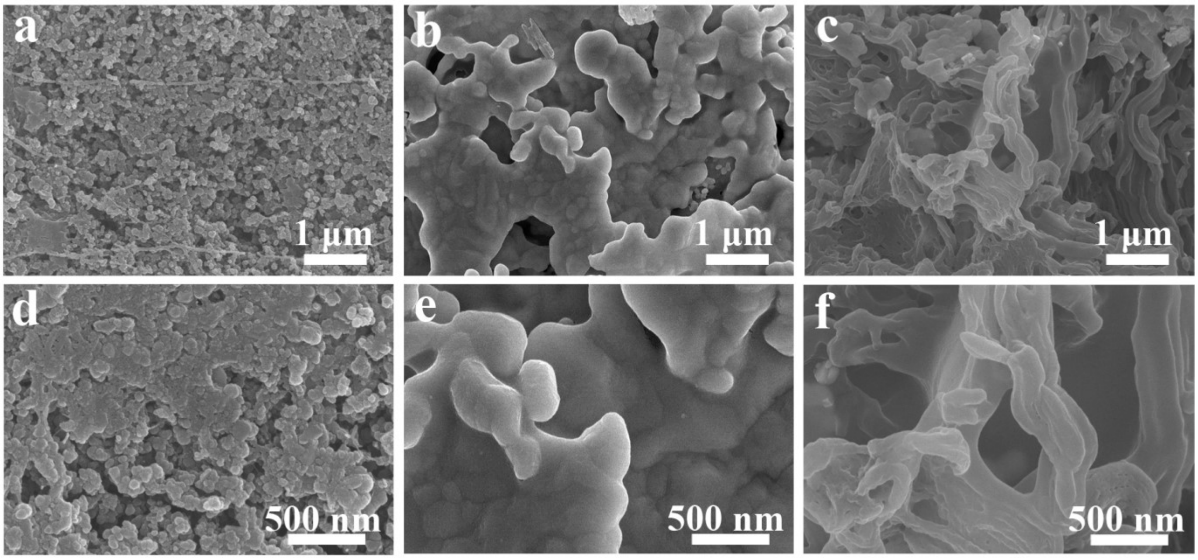

Figure S2. SEM images of (a, d) CP, (b, e) Ag/CP, and (c, f) p-Ag/CP.

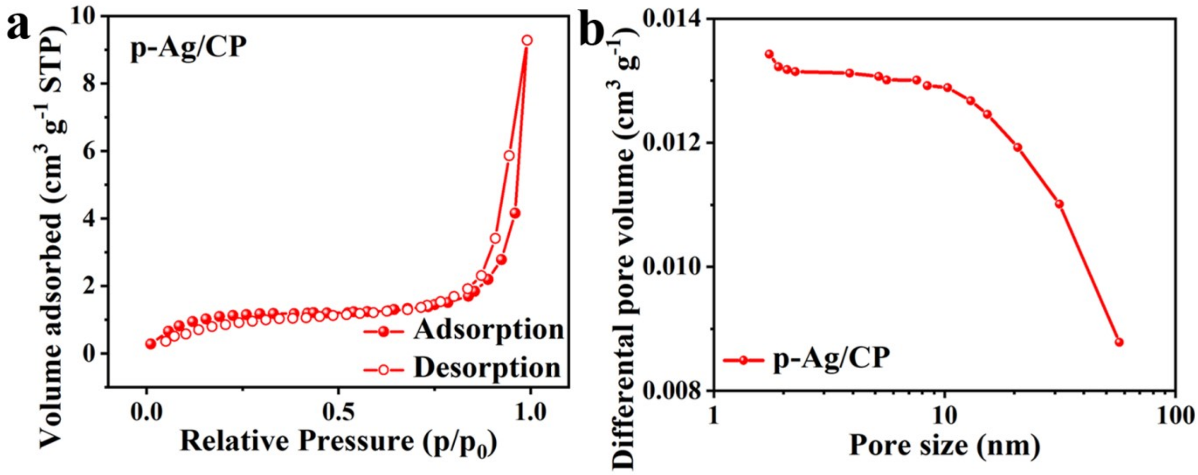

Figure S3. (a) The nitrogen sorption isotherms at 77 K (closed, adsorption; open, desorption) and (b) corresponding pore size distribution curves for p-Ag/CP.

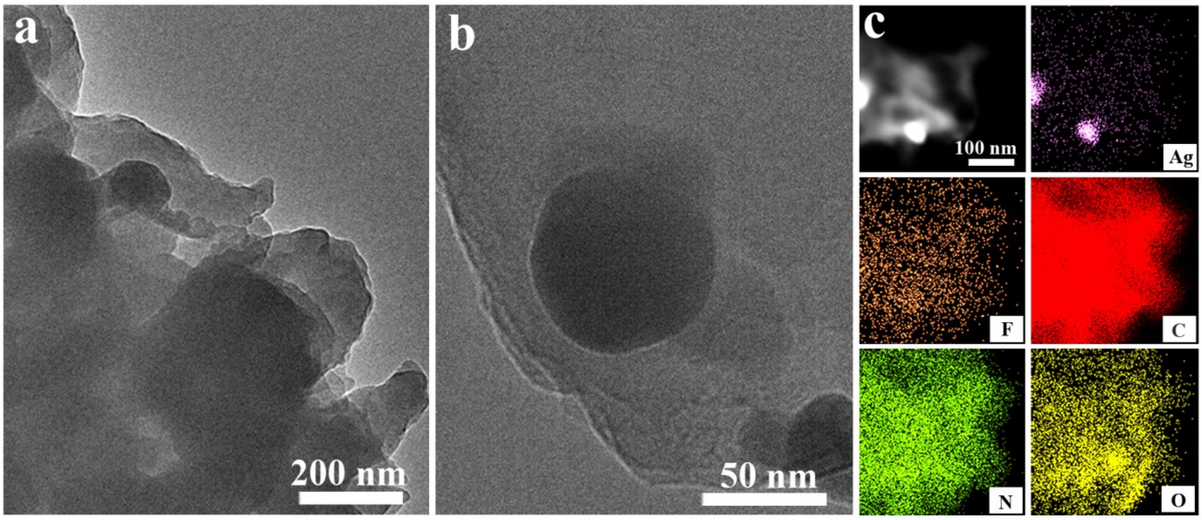

Figure S4. (a, b) TEM and (c) elemental mapping images of p-Ag/CP.

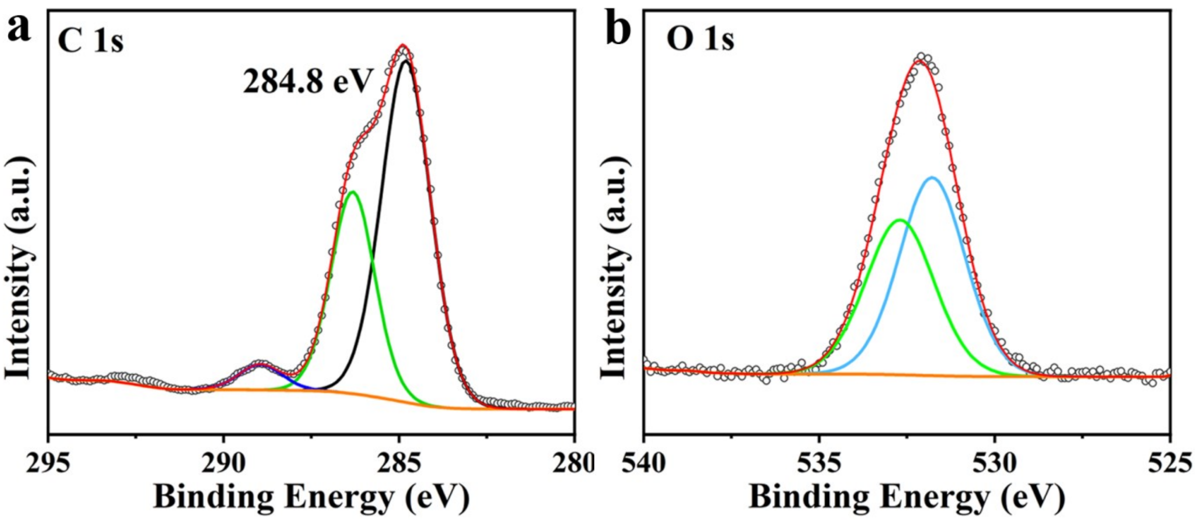

Figure S5. High-resolution XPS spectrum (a) C 1s and (b) O 1s of p-Ag/CP.

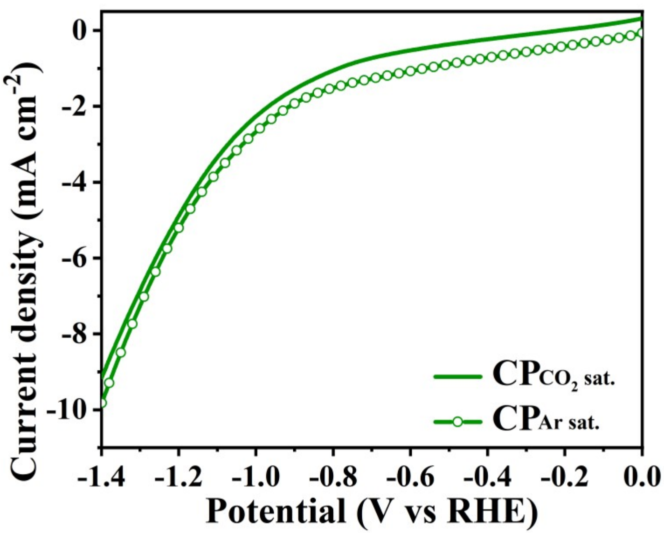

Figure S6. LSV curves (5 mV s^{-1}) for the CP in Ar- and CO_2-saturated 0.1 M $KHCO_3$ solution.

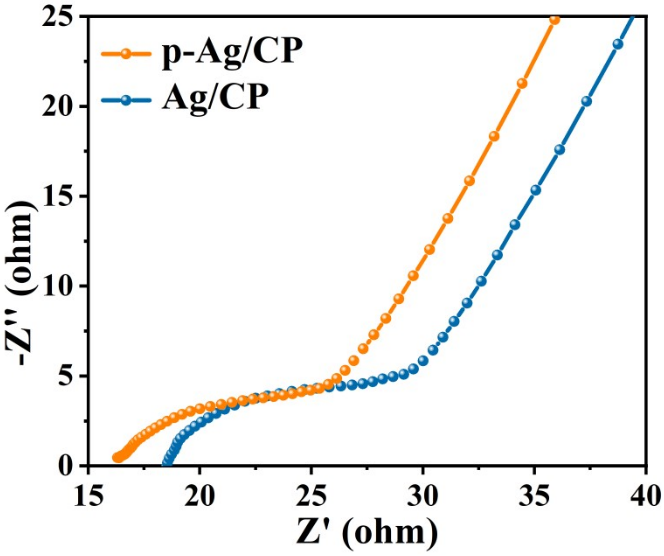

Figure S7. Nyquist diagrams of the Ag/CP and p-Ag/CP.

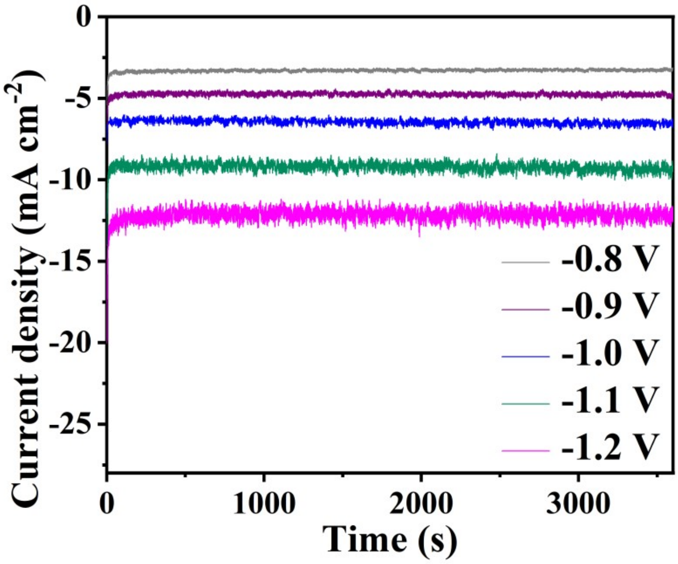

Figure S8. The i-t test results of p-Ag/CP in CO_2RR.

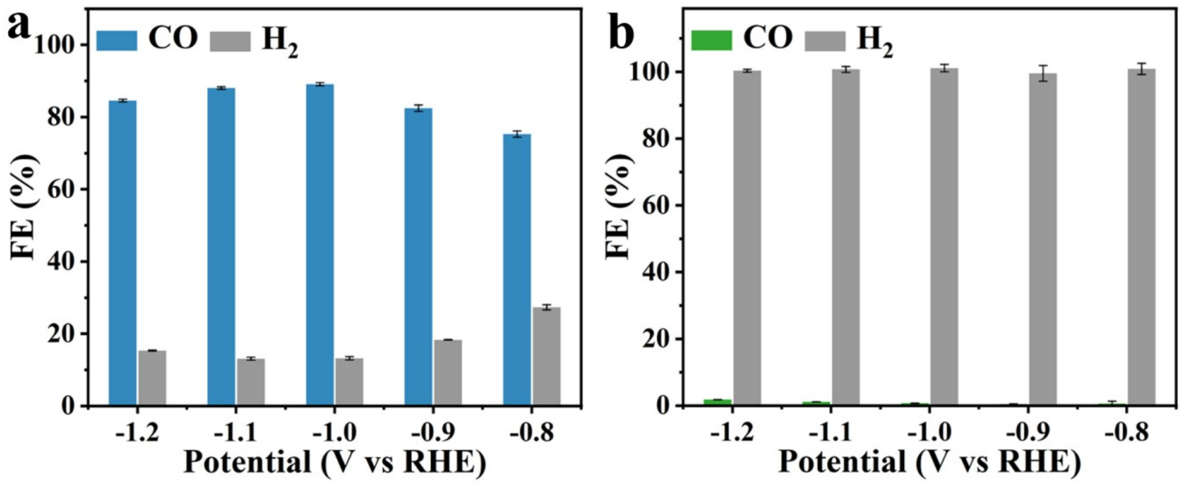

Figure S9. FE_{CO} value of (a) Ag/CP and (b) CP at various applied potentials.

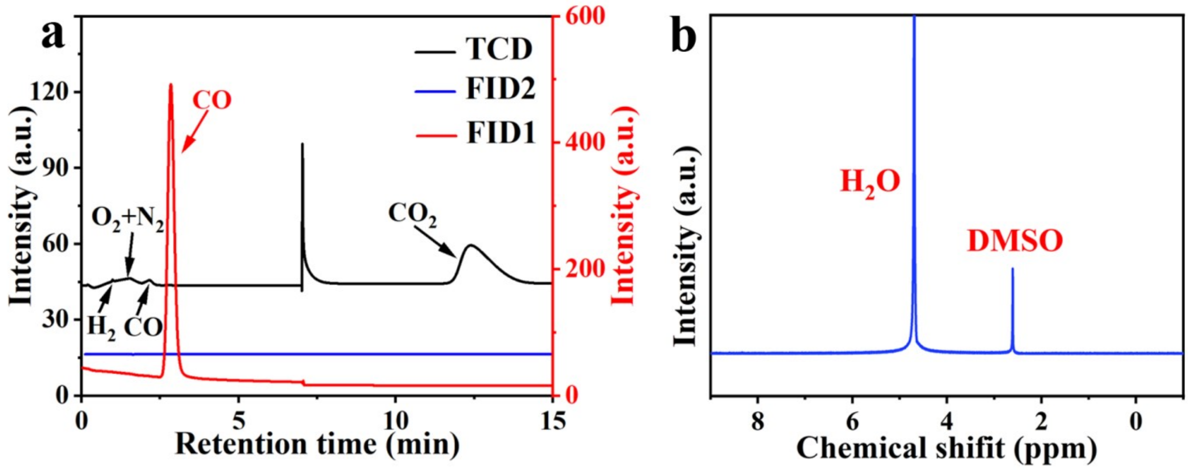

Figure S10. (a) GC curves of the CO_2RR gas product for p-Ag/CP at -1.0 V vs RHE. Only main CO and trace amounts of H_2 can be detected as a reduction product for both TCD and FID channels. (b) ^{1}H NMR spectrum of the CO_2RR liquid product for p-Ag/CP at -1.0 V vs RHE. The DMSO was added as an internal standard, and no liquid reduction product can be detected.

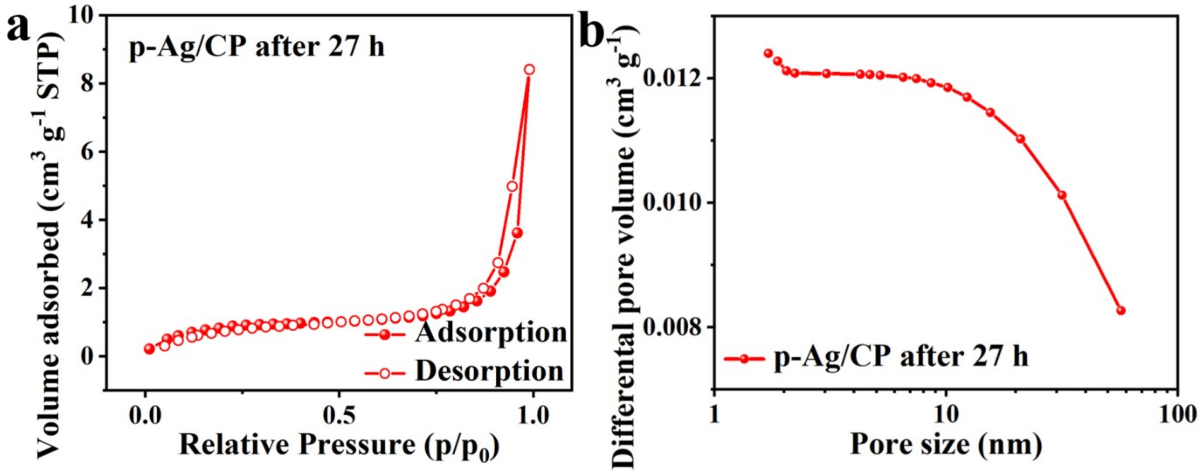

Figure S11. (a) The nitrogen sorption isotherms at 77 K (closed, adsorption; open, desorption) and (b) corresponding pore size distribution curves for p-Ag/CP after CO_2RR stability test. The obtained BET specific surface area of p-Ag/CP after CO_2RR stability test is 3.42 m^2 g^{-1}.

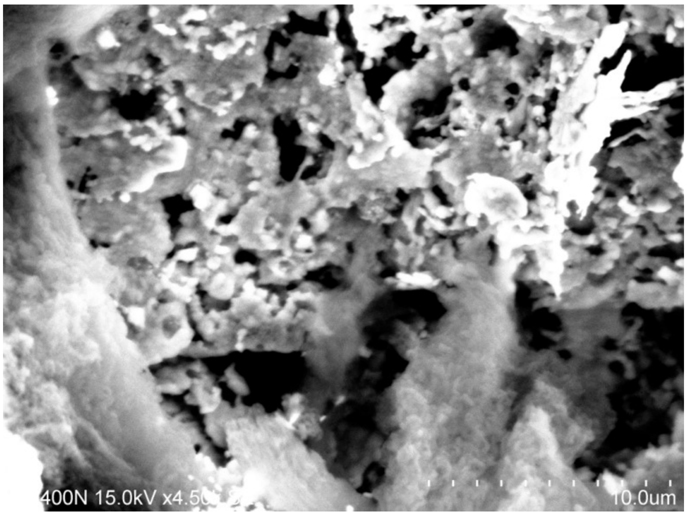

Figure S12. SEM image of p-Ag/CP after CO_2RR stability test.

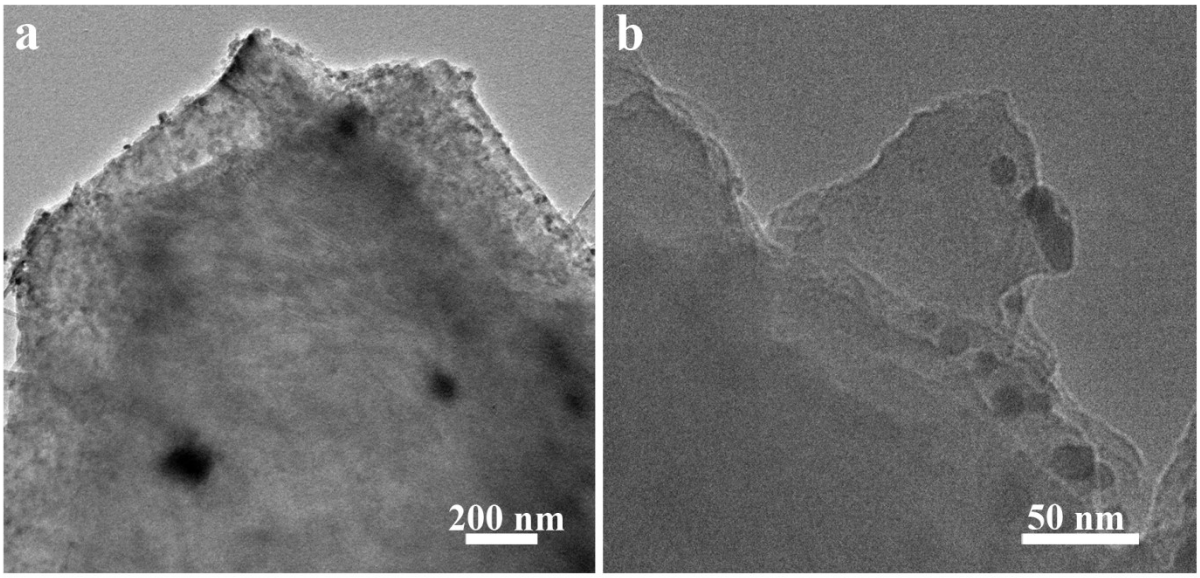

Figure S13. TEM image of p-Ag/CP after CO_2RR stability test.

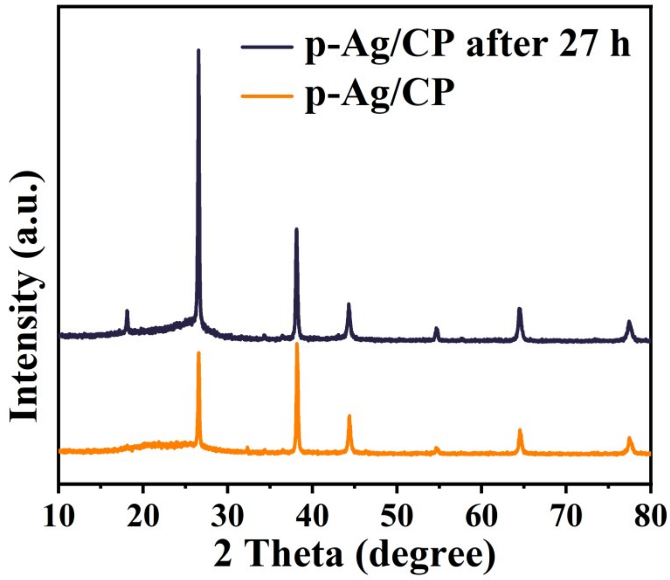

Figure S14. XRD patterns of p-Ag/CP before and after CO_2RR stability test.

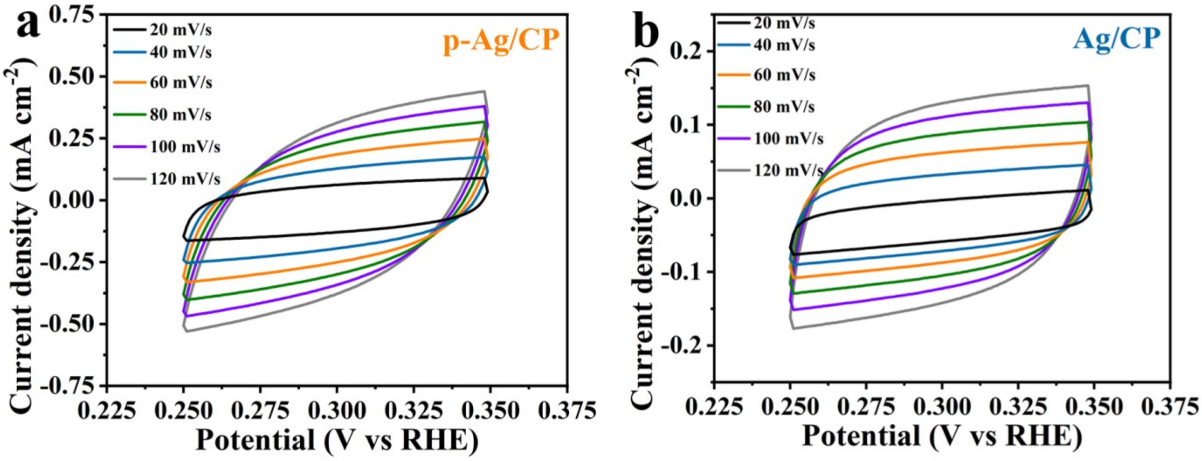

Figure S15. CV curves of p-Ag/CP and Ag/CP in non-Faradaic regions.

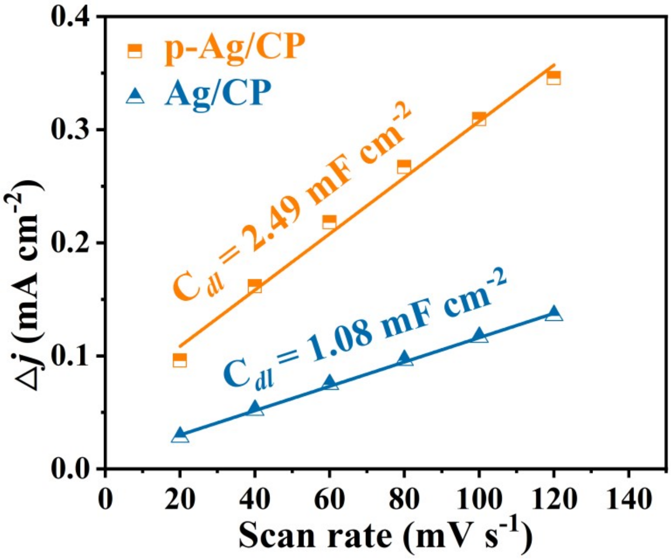

Figure S16. The C_{dl} values of p-Ag/CP and Ag/CP samples.

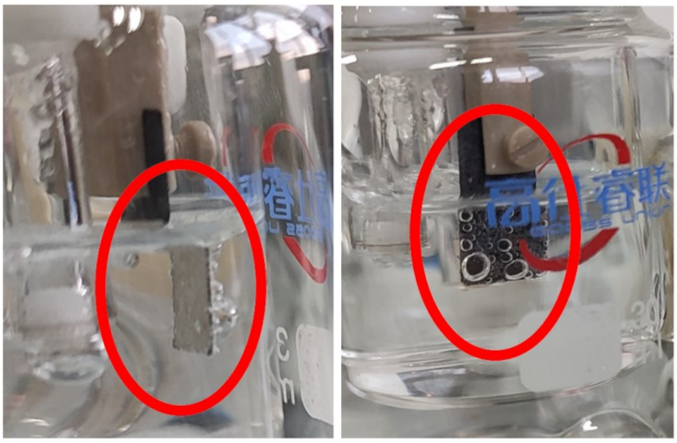

Figure S17. The optical picture for surface of p-Ag/CP in the CO_2RR.

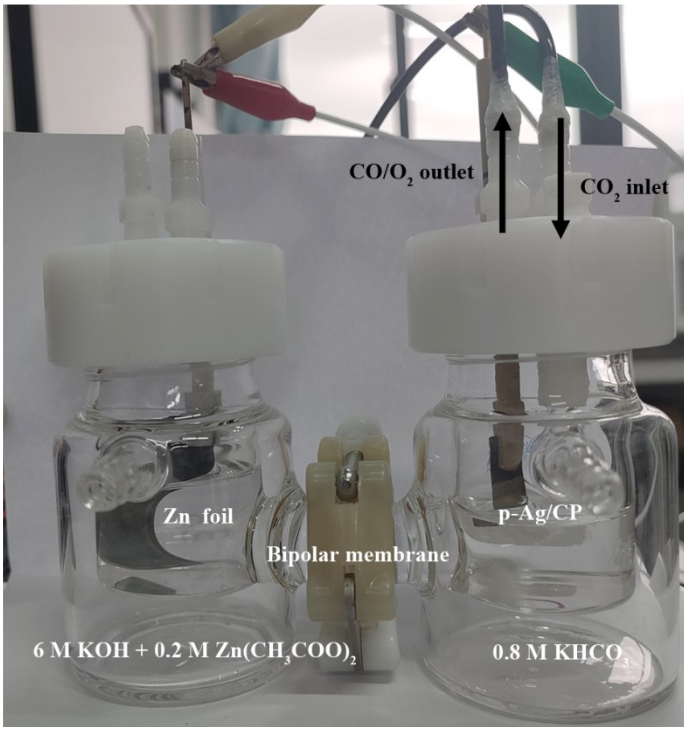

Figure S18. The optical picture of assembled Zn-CO_2 battery with p-Ag/CP cathode.

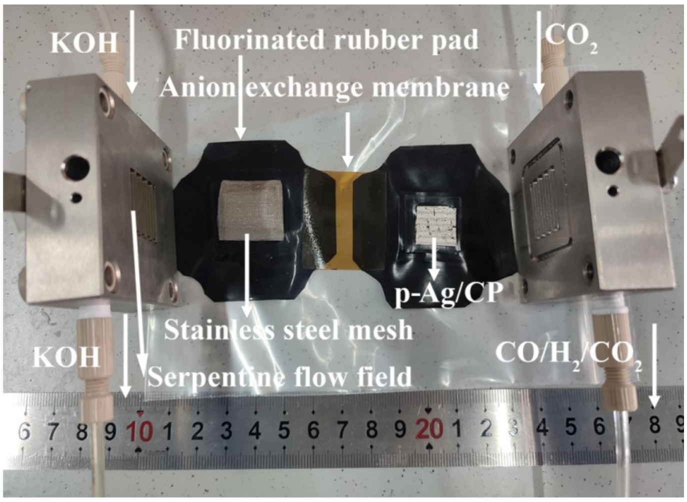

Figure S19. The optical picture of MEA for CO_2RR.

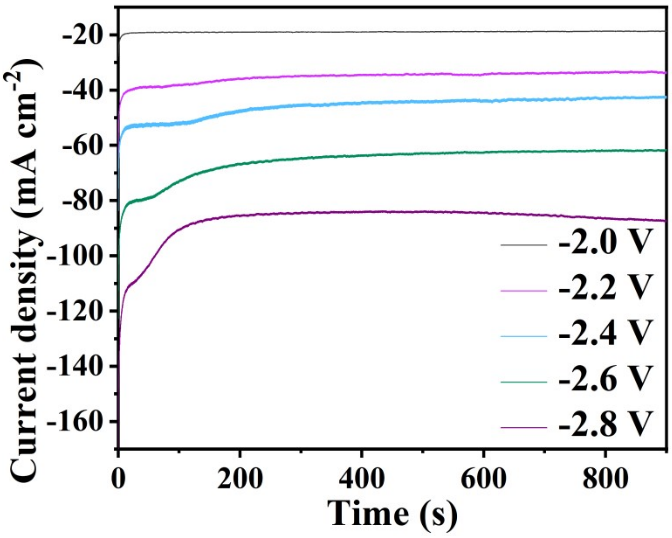

Figure S20. The i-t test results of p-Ag/CP in MEA.

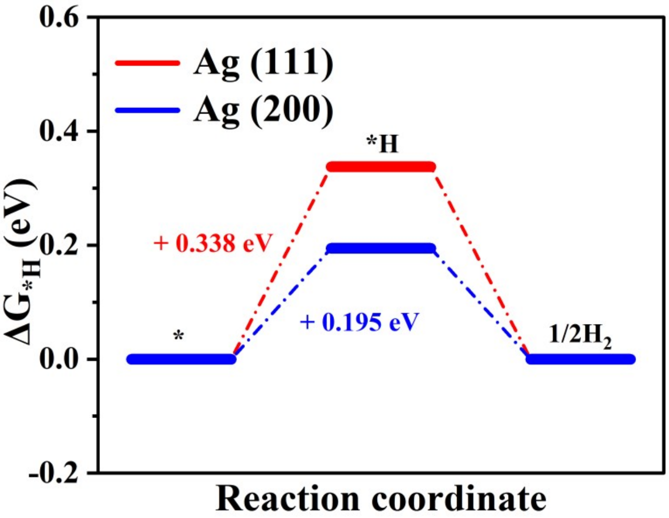

Figure S21. The calculated free energy profile of p-Ag/CP for HER.

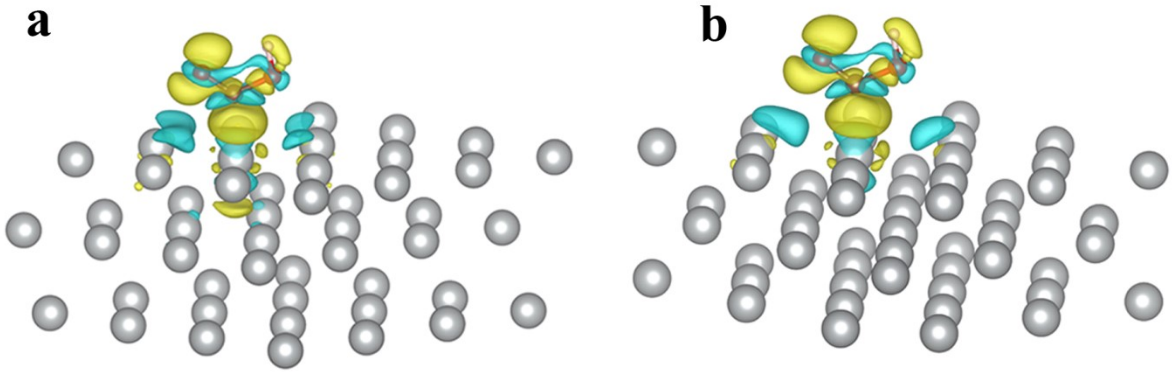

Figure S22. Charge density differences of *COOH on (a) Ag (111) and (b) Ag (200) surface of p-Ag/CP. Note that yellow and cyan regions represent electron accumulation and loss, respectively.

Table S1. The element content of p-Ag/CP obtained via the EDX spectroscopy.

Element	Line	Intensity (c/s)	Content	Units	Error 2-sig	MDL 3-sig	
C	Ka	394.35	5.026	wt.%	0.164	0.053	
N	Ka	0.99	0.074	wt.%	0.221	0.331	
O	Ka	11.81	0.119	wt.%	0.041	0.053	
F	Ka	0.70	0.024	wt.%	0.137	0.208	
Ag	La	1,498.41	94.758	wt.%	1.665	0.939	
			100.000	wt.%			Total

Table S2. The element content of p-Ag/CP after CO_2RR stability test obtained via the EDX spectroscopy.

Element	Line	Intensity (c/s)	Content	Units	Error 2-sig	MDL 3-sig	
C	Ka	219.77	2.868	wt.%	0.125	0.041	
N	Ka	5.92	0.446	wt.%	0.201	0.252	
O	Ka	5.10	0.050	wt.%	0.027	0.035	
F	Ka	0.00	0.000	wt.%	0.000	0.000	
Ag	La	1,499.72	96.635	wt.%	1.680	0.884	
			100.000	wt.%			Total

Table S3. Summary of the CO Faradaic efficiency, potential and stability towards CO_2 reduction reaction from reported electrocatalysts.

Catalysts	FE_{CO} (%)	Potential (V vs RHE)	Stability	Reference
p-Ag/CP	>94.0	-1.0	27 h	This work
Fe-SA/BNC	94	-0.7	30 h	[1]
NSHPC	88	0.49	10	[2]
Ag-200 nm NWA	91	-0.6	2 h	[3]
SD-AgPMR-30	60	0.56	10 h	[4]
Ag-NCs	~95	0.746	18	[5]
$Zn-N_4$	95	0.32	75	[6]

Reference

[1] S. Liu, M. Jin, J. Sun, Y. Qin, S. Gao, Y. Chen, S. Zhang, J. Luo, X. Liu, Coordination environment engineering to boost electrocatalytic CO_2 reduction performance by introducing boron into single-Fe-atomic catalyst, Chem. Eng. J., 2022, 437, 135294, http://doi.org/10.1016/j.cej.2022.135294.
[2] R. Li, F. Liu, Y. Zhang, M. Guo, D. Liu, Nitrogen, Sulfur Co-Doped Hierarchically Porous Carbon as a Metal-Free Electrocatalyst for Oxygen Reduction and Carbon Dioxide Reduction Reaction, ACS Appl. Mater. Interfaces, 2020, 12(40), 44578-44587, http://doi.org/10.1021/acsami.0c06506.
[3] C. Luan, Y. Shao, Q. Lu, S. Gao, K. Huang, H. Wu, K. Yao, High-Performance Carbon Dioxide Electrocatalytic Reduction by Easily Fabricated Large-Scale Silver Nanowire Arrays, ACS Appl. Mater. Interfaces, 2018, 10(21), 17950-17956, http://doi.org/10.1021/acsami.8b03461.
[4] J. Yang, H. Du, Q. Yu, W. Zhang, Y. Zhang, J. Ge, H. Li, J. Liu, H. Li, H. Xu, Porous silver microrods by plasma vulcanization activation for enhanced electrocatalytic carbon dioxide reduction, J. Colloid Interface Sci., 2022, 606, 793-799, http://doi.org/10.1016/j.jcis.2021.08.061.
[5] S. Liu, C. Sun, J. Xiao, J.-L. Luo, Unraveling Structure Sensitivity in CO_2 Electroreduction to Near-Unity CO on Silver Nanocubes, ACS Catal., 2020, 10(5), 3158-3163, http://doi.org/10.1021/acscatal.9b03883.
[6] F. Yang, P. Song, X. Liu, B. Mei, W. Xing, Z. Jiang, L. Gu, W. Xu, Highly Efficient CO_2 Electroreduction on ZnN4-based Single-Atom Catalyst, Angew. Chem. Int. Ed., 2018, 57(38), 12303-12307, http://doi.org/10.1002/anie.201805871.